Neutron News
Publication details, including instructions for authors and subscription information:
http://www.tandfonline.com/loi/gnnw20

Characterization of Zr-based nuclear components by TOF neutron diffraction

J. R. Santisteban[a], M. A. Vicente Álvarez[a], F. Malamud[a], P. Vizcaíno[b] & W. Kockelmann[c]
[a] Centro Atómico Bariloche, CNEA and CONICET, Bariloche, 8400, Argentina
[b] Centro Atómico Ezeiza, CNEA and CONICET, Ezeiza, 1802, Argentina
[c] Rutherford Appleton Laboratory, ISIS Facility, Chilton, OX11 0QX, United Kingdom
Published online: 30 Oct 2014.

Characterization of Zr-based nuclear components by TOF neutron diffraction

J. R. Santisteban[1], M. A. Vicente Álvarez[1], F. Malamud[1], P. Vizcaíno[2], and W. Kockelmann[3]
[1]Centro Atómico Bariloche, CNEA and CONICET, Bariloche, 8400, Argentina
[2]Centro Atómico Ezeiza, CNEA and CONICET, Ezeiza, 1802, Argentina
[3]Rutherford Appleton Laboratory, ISIS Facility, Chilton, OX11 0QX, United Kingdom

Zr-2.5%Nb pressure tubes are important components of CANDU nuclear power plants. In-reactor performance depends on a number of microstructural parameters such as crystallographic texture, dislocation densities and volume of minority phases. Neutron diffraction experiments can be used to follow the variation of such parameters at different stages of manufacturing processes. Here we report recent measurements carried out on ENGIN-X (a time-of-flight neutron diffractometer at the ISIS Facility, United Kingdom), to characterize a novel processing scheme recently developed in Argentina. An optimized measurement strategy resulted in reduced experimental times to complete the study.

Introduction

Due to its good mechanical strength, corrosion and creep resistance, and excellent neutronic properties, Zr–2.5%Nb is used as the pressure tube material in CANDU nuclear power plants. The in-service performance of the pressure tubes is strongly dependent on texture, microstructure and intergranular residual stresses, which are controlled by the manufacturing schedule [1]. Starting from forged Zr–2.5%Nb billets, the general fabrication route of CANDU pressure tubes consists of i) extrusion at ~800°C, followed by air cooling, ii) cold drawing to ~20–30% strain and, iii) autoclaving at 400°C for 24 h. After extrusion, the material consists of ~90% *hcp* a-Zr, and ~10% metastable *bcc* β-Zr, which contains approximately 20% Nb. During autoclaving, β-Zr partially transforms to β-Nb (~95% Nb) and contains a metastable w-phase and an enriched β-Zr phase (~50%Nb). In finished tubes, the volume fraction and composition of β-Zr phase, and the texture and density of dislocations of the α-Zr phase, are important variables carefully specified by the designer. In Argentina, Argentina Atomic Energy Commission (CNEA) has developed a slightly different processing schedule which starts from the extruded tubes and replaces the cold-drawing stage by a cold-rolling stage. Although the tube deformation introduced in both cases are equivalent (~20–30% strain), differences in starting material and deformation processes suggest that dislocation densities, residual stresses and texture profiles of finished tubes would not be identical. In order to characterize this processing schedule, we have measured dislocation densities and crystallographic texture of the main α-Zr phase, and composition of minority phases by time-of-flight (TOF) neutron diffraction experiments.

Experiments

Studies were performed on small coupons produced after three manufacturing stages: i) extrusion, ii) cold-rolling, and iii) autoclaving (heat-treatment). TOF diffraction experiments were done on the ENGIN-X diffractometer, United Kingdom [2]. Two diffraction banks centred at Bragg angles $2\theta = \pm 90°$ allowed measuring full TOF-diffraction patterns along two perpendicular directions of the sample simultaneously. The coupons were fitted into a goniometer to record TOF diffractograms at different specimen orientations, and hence quantify the crystallographic texture. Just four orientations were measured for each coupon, carefully chosen to provide information from the most important regions of pole figures, for both *basal* (0002), and *prismatic* (10-10) planes of the α-Zr *hcp* structure. This also ensured good averaging of dislocation densities for such anisotropic specimens. The usually narrow incident beam divergence of the instrument was relaxed to reduce counting times, so the full study (3 specimens × 4 orientations) was completed in less than two hours.

Results

Crystallographic phases

Figure 1 shows diffractograms obtained for the different manufacturing stages, where the main crystallographic phases have been indexed. For better sampling,

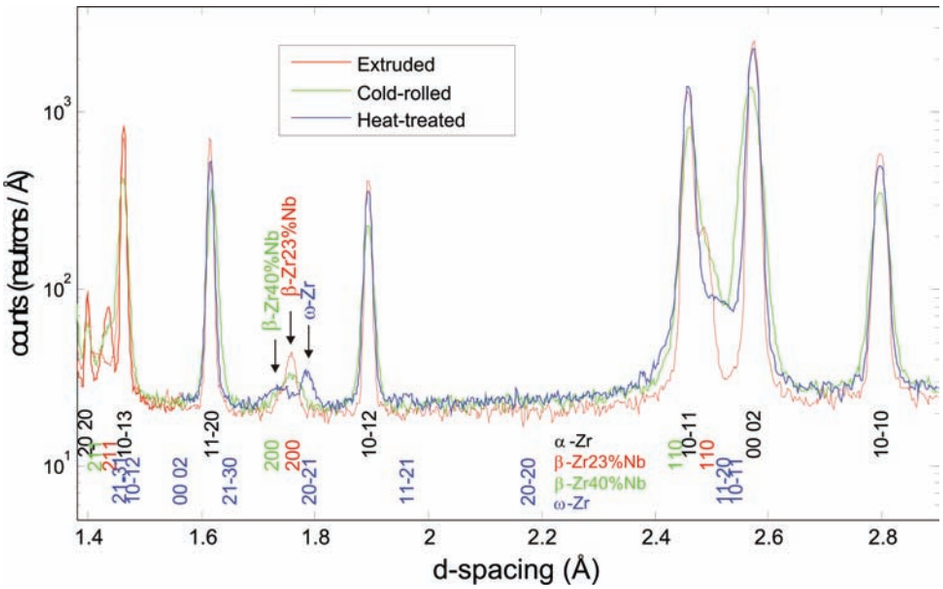

Figure 1. Bulk diffractograms for specimens from the different manufacturing stages.

data recorded by different banks and at different orientations were binned into single diffractograms. As expected, all three diffractograms look very similar, with the α-Zr phase dominating the pattern, although with slightly broader peaks observed for the cold-worked material. Microstructural differences reveal mainly through changes in the minority phases. The extruded material displays sharp (200), (211), (110) peaks from the β-Zr phase of a composition of ~23% Nb ($\beta_{23\%}$ phase). The composition was calculated from Veegard's law for the ZrNb system [3]. The $\beta_{23\%}$ phase is also observed in the cold-worked material, with the peaks substantially broader due to the 28% cold deformation. After heat treatment, the $\beta_{23\%}$ phase decomposes into a β-Zr phase with a composition of ~40% Nb and the ω-Zr phase. The $\beta_{40\%}$(200) peak appears much broader than the ω(20-21) peak. On the other hand, the α-Zr peaks become sharper, although slightly broader and less intense than those of the extruded material.

Texture and Kearns factors

The texture of Zr-2.5%Nb pressure tubes is very strong and mainly defined at the extrusion stage [4]. In manufacturing, texture is specified through the Kearns factors [5], parameters assessing the proportion of *c*-axes that are projected along the tube three principal axes. They are calculated from basal (0002) pole figures.

$$f_z = \int_0^{\pi/2} I_{(0002)}(\varphi) \sin\varphi \cos^2\varphi \, d\varphi,$$

where *z* is the direction of interest in the tube (f_H, f_R, f_A for hoop, radial or axial, respectively); and $I_{(0002)}(\varphi)$ sin φ is the fraction of crystals having their *c*-axis at an angle φ from that direction. As shown by the experimental (0002) pole figure in the inset of Figure 2, here we have measured very incomplete pole figures, i.e., only along the hoop-radial line, and around the axial direction. Yet, these are the most relevant regions, where differences introduced by the manufacturing process manifest more clearly. To produce such pole figure, we have split ENGIN-X diffraction banks into smaller sub-units covering

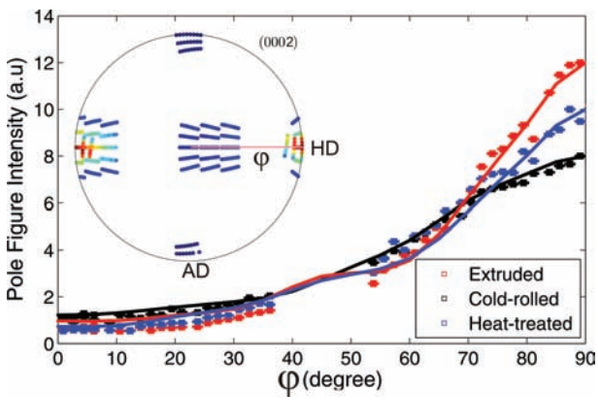

Figure 2. Experimental pole figures along the hoop-radial direction recorded for the three specimens. Solid lines are calculated values from the refined ODFs.

Table 1. Results of present analysis: $\langle\varepsilon^2\rangle^{1/2}$: mean-square strain, ΔK_0: intercept of W-H plot.

Sample	Kearns factor (±0.02)			$\langle\varepsilon^2\rangle^{1/2}$	ΔK_0	Dislocation density [$\times 10^{14}$ m^{-2}]		
	Hoop	Radial	Axial	[με]	[10^{-4} Å^{-1}]	ρ_a	ρ_c	$\rho_a + \rho_c$
Extruded	0.564	0.361	0.073	330	3.2	0.1	0.04	0.14
Cold-rolled	0.618	0.288	0.091	1200	2.2	9.2	1.8	11.0
Heat-treated	0.556	0.335	0.108	640	2.4	1.3	0.36	1.66

reduced solid angles, as recently described in Reference [6]. Details of the hoop-radial line of the (0002) pole figure for the three specimens are shown by the symbols in the main plot of Figure 2. From four experimental pole figures as the one in the inset {(10-10), (0002), (10-11) and (10-12)}, we determined the orientation distribution function (ODF) for each sample using the MTEX algorithm [6,7]. Solid lines in the plot show the recalculated pole figures along the hoop-radial directions. Table 1 lists the Kearns factors evaluated from such recalculated pole figures. Results for the final product, i.e, the heat-treated specimen, agree very well with those obtained by other techniques [8].

Dislocation densities

Regarding dislocation densities, designers specify maximum numbers for *a*-type and *c*-type dislocations, as they evolve differently upon irradiation. Dislocations and other lattice defects manifest through broadening of diffraction peaks. For quantification, the most simple analysis is that of Williamson and Hall (W-H) [9], in which the *physical* broadening is analyzed in the reciprocal space using the variable $K = 1/d$, where d is the interplanar distance corresponding to each peak. Figure 3 shows W-H plots obtained for the three specimens. Using Gaussian profiles, the physical broadening was calculated from the observed broadening as $\sigma_{phys} = (\sigma^2_{obs} - \sigma^2_{instr})^{1/2}$, with σ_{instr} the (interpolated) width measured for a CeO_2 reference powder. The extruded and heat-treated specimens display reasonably linear behavior, although deviations from a straight line are much higher than the uncertainty of measured points. For the cold-rolled specimen such deviations are ~20% and a linear dependence is not evident. The slope (m) obtained by a least-squares fit gives a measure of the mean-square strain in the material, $\langle\varepsilon^2\rangle^{1/2} = m/\sqrt{2\pi}$ [9]. The values obtained for the three specimens are listed in Table 1. The intersection of the DK curves with the origin (ΔK_0) is defined by the average grain size of the material. In the present case, the intercept of all three least-squares lines are $\Delta K_0 \sim 0.0002$ Å^{-1}, indicating rather large grain sizes that would be difficult to define by this technique. This conclusion is valid even considering that for the Gaussian peak shapes observed here the ΔK curves should flatten near the origin.

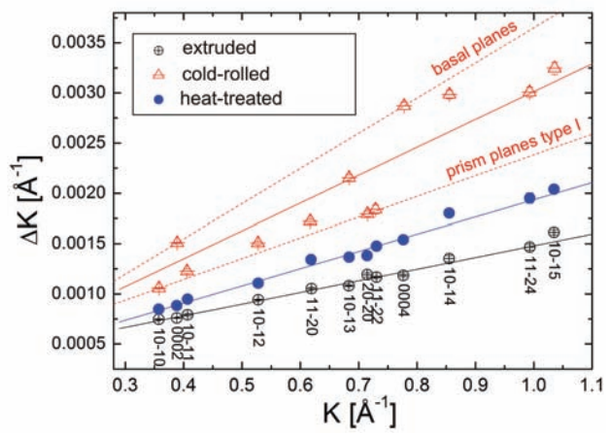

Figure 3. Williamson-Hall plot of the physical peak broadening measured for the three samples.

An estimation of the density of dislocations within the material can be obtained by assuming that the observed mean-square strains are exclusively due to dislocations. For isotropic distributions of dislocations, the dislocation density can be calculated as $= A\langle\varepsilon^2\rangle^{1/2}/b^2$, with b the Burgers vector and A a constant that includes details of the dislocation type [10]. For anisotropic distributions of dislocations as found in *hcp* α-Zr, this equation needs to be modified to differentiate type-*a* and type-*c* component dislocations. In the present analysis we have followed the assumptions in Reference [11], which give

$$\rho_c = \langle\varepsilon^2\rangle_c \, 10^{20} \text{ m}^{-2},$$
$$\rho_a = 5\langle\varepsilon^2\rangle_a \, 10^{20} \text{ m}^{-2},$$

with $\langle\varepsilon^2\rangle_c$ and $\langle\varepsilon^2\rangle_a$ the mean-square strains obtained for the basal (0001) and prism (10-10 and 11-20) planes of the hexagon respectively. Dislocations densities obtained for the three specimens are listed in Table 1. As indicated in Figure 3 for the cold-rolled specimen, the slope given by the basal (0002) and (0004) peaks was used to de-

fine $\langle \varepsilon^2 \rangle_c$, whilst the slope from the (10-10) and (20-20) prism peaks was used for $\langle \varepsilon^2 \rangle_a$. The reported dislocation densities are within the values expected for this material in these microstructural conditions [12]. The values for the heat-treated coupon lie within the specifications for the final product. More sophisticated analyses based on a modified Warren-Averbach method have also been applied [13], but details of such procedure are beyond the scope of this work.

Conclusions

Subtle microstructural changes occur during manufacturing of Zr-2.5%Nb pressure tubes, which must be properly controlled in order to satisfy design specifications. Neutron diffraction with a polychromatic neutron beam allowed a detailed characterization of such changes in specimens produced at three stages of the manufacturing process: after extrusion, after 28% cold-rolling and after an autoclaving heat treatment. Microstructural changes manifested through small changes in the intensity and broadening of diffraction peaks from the main α-Zr phase; and by substantial changes in the composition and crystal structure of secondary phases (β-Zr and ω-Zr). Variations in texture were quantified in terms of the ODF of crystallites, and by Kearns factors, the operational variable used in manufacturing. A modified Williamson-Hall analysis of the variations observed in peak width allowed quantification of type-*a* and type-*c* dislocation densities. Both Kearns factors and dislocation densities of the final product were within the ranges specified for pressure tubes. The optimized measurement strategy described here (~30 minutes per sample) can be used as a guideline for efficient characterization of Zr based components in TOF neutron strain scanners.

References

1. R. A. Holt, *J. Nuclear Materials* **372**, 182–214 (2008).
2. J. R. Santisteban, M. R. Daymond, J. A. James, L. Edwards, *J. Applied Crystallography* **39**, 812–825 (2006).
3. G. Aurelio, A. F. Guillermet, G. J. Cuello, J. Campo, *Metall. Materials Transactions* **A32**, 1903–1910 (2001).
4. R. A. Holt and S. A. Aldridge, *J. Nuclear Materials* **135**, 246–259 (1985).
5. J. J. Kearns, *J. Nuclear Materials* **299**, 171–174 (2001).
6. F. Malamud, J. R. Santisteban, M. A. Vicente Alvarez, R. Bolmaro, J. Kelleher, S. Kabra, W. Kockelmann, *J. Applied Crystallography* **47** (4), 1337–1354 (2014).
7. R. Hielscher and H. Schaeben, *J. Applied Crystallography* **41**, 1024–1037 (2008).
8. IAEA TecDoc: Use of Neutron Beams for Materials Research Relevant to Nuclear Energy Sector, International Atomic Energy Agency, Vienna, 2014 (in press).
9. G. K. Williamson and W. H. Hall, *Acta Metallurgica* **1**, 22–31 (1953).
10. G. K. Williamson and R. E. Smallman, *Philos. Mag.* **1**, 34 (1956).
11. J. E. Winegar, AECL Technical Report CRNL-4098 (1987).
12. L. Balogh, D. W. Brown, P. Mosbrucker, F. Long, M. R. Daymond, *Acta Materialia* **60**, 5567–5577 (2012).
13. T. Ungár, J. Gubicza, G. Ribárik, and A. Borbély, *J. Applied Crystallography* **34** (3), 298–310 (2001).